



## Phase transitions and magnetic properties of Fe<sub>30</sub>Co<sub>29</sub>Ni<sub>29</sub>Zr<sub>7</sub>B<sub>4</sub>Cu<sub>1</sub> high-entropy alloys



Ran Wei<sup>a</sup>, Hang Zhang<sup>a</sup>, Hongyan Wang<sup>a</sup>, Chen Chen<sup>a</sup>, Tan Wang<sup>a</sup>, Fushan Li<sup>a,\*</sup>, Shaokang Guan<sup>a</sup>, Tao Zhang<sup>b</sup>, Tingwei Hu<sup>c</sup>, Yaqiang Dong<sup>d</sup>

<sup>a</sup> School of Materials Science and Engineering, Zhengzhou University, Zhengzhou 450001, China

<sup>b</sup> Key Laboratory of Aerospace Materials and Performance (Ministry of Education), School of Materials Science and Engineering, Beihang University, Beijing 100191, China

<sup>c</sup> State Key Laboratory for Mechanical Behavior of Materials, Xi'an Jiaotong University, Xi'an 710049, China

<sup>d</sup> Zhejiang Province Key Laboratory of Magnetic Materials and Application Technology, Key Laboratory of Materials and Devices, Ningbo Institute of Materials Technology and Engineering, Chinese Academy of Sciences, Ningbo 315201, China

### ARTICLE INFO

#### Article history:

Received 7 January 2019

Received in revised form

6 March 2019

Accepted 7 March 2019

Available online 8 March 2019

#### Keywords:

High entropy alloys

Amorphous materials

Magnetic properties

Phase transitions

Computer simulations

### ABSTRACT

Phase transitions are widely observed in many metal materials including amorphous alloy and high-entropy alloys (HEAs). When HEAs are made in the amorphous form, is it possible for the amorphous phase to transition to simple solid solution? This paper reveals a phase transition from amorphous phase to body-centered cubic (bcc) phase and then to face-centered cubic (fcc) phase in Fe<sub>30</sub>Co<sub>29</sub>Ni<sub>29</sub>Zr<sub>7</sub>B<sub>4</sub>Cu<sub>1</sub> HEA by employing simple heat treatment process. Accordingly, the intrinsic correlation between the microstructure and soft-magnetic properties was established by excluding the composition interference. The explanation of mechanism behind the phase transitions was explored by first-principles density functional theory (DFT) calculations and other methods. This research suggests an approach of designing HEAs with excellent magnetic properties, and provides a prototype to study structure of amorphous alloys.

© 2019 Elsevier B.V. All rights reserved.

### 1. Introduction

Phase transitions with identical compositions have attracted considerable attention in recent years [1–7]. Pressure and temperature are usually two controlling parameters in phase transition. Pressure-induced phase transformation was widely studied. Pressure-induced phase transition from magnetic hcp (hexagonal close-packing) phase to nonmagnetic fcc (face-centered cubic) phase in Co was reported [5]. Pressure-induced structure transitions in Fe also yield the loss of ferromagnetic behavior [1,5]. In addition, pressure-induced amorphous to fcc phase transition was found in Ce<sub>75</sub>Al<sub>25</sub> amorphous alloy [7]. As an important external parameter, the temperature-induced phase transitions is also an ubiquitous phenomenon. The bcc (body-centered cubic) and fcc forms of Fe with increasing temperature are a familiar example of phase transitions [6].

Recently, high-entropy alloys (HEAs), consisting of five or more

principal elements in equal or near-equal atomic percent, have attracted attentions by breaking the traditional alloy design concept [8–10]. Rather than forming intermetallic phase, HEAs usually tend to form amorphous, fcc or bcc structures [11]. Owing to their unique structures, HEAs are potential materials to coupling good mechanical properties of crystal structure and excellent physical properties of amorphous structure [9,12]. Our previous research shows that Fe–Co–Ni–Si–B HEA possesses good ductility and soft-magnetic properties, which is due to its ability to form amorphous-HEAs or fcc-HEAs depending on the preparation process [13,14]. There is reason to conjecture that phase structure affect the magnetic properties of HEAs. However, when researchers study the effects of structures on magnetic behavior of HEAs, they usually focus on altering the compositions, limiting the understanding of the intrinsic magnetic mechanism [15–17]. Up to now, HEAs with amorphous, bcc or fcc phase structure in alike compositions have not been prepared yet. More recently, pressure or stress induced phase transition was found in HEAs [1,3,4,18]. This invites the question: would temperature-induced phase transformation ever occur in amorphous-HEAs?

\* Corresponding author.

E-mail address: [fsli@zzu.edu.cn](mailto:fsli@zzu.edu.cn) (F. Li).

In this work, we employed a simple crystallization technique and discovered a phase transition from amorphous to bcc and then to fcc in  $\text{Fe}_{30}\text{Co}_{29}\text{Ni}_{29}\text{Zr}_7\text{B}_4\text{Cu}_1$  HEA with increasing temperature. First-principles density functional theory (DFT) calculations reveal that the average cohesive energy per atom of amorphous and bcc phase is very close to each other ( $-5.17788$  eV and  $-5.17429$  eV), while the fcc phase has relatively high cohesive energy per atom of  $-5.1657$  eV. The saturation magnetization ( $B_s$ ) of the HEAs with bcc structure is higher than that of amorphous, while  $B_s$  of the amorphous phase is approximately equal to that of fcc phase, because the magnetic momentum of bcc, amorphous and fcc phase is 1.294, 1.246 and 1.239  $\mu_B/\text{atom}$  derive by DFT calculations, respectively. This discovery offers a new perspective for understanding the structure evolution and magnetic properties of HEAs, and provides a prototype for designing HEAs with excellent soft magnetic properties. Our work opens a new avenue to study the microstructure of high entropy amorphous alloys.

## 2. Methods

Alloy ingots with nominal composition of  $\text{Fe}_{30}\text{Co}_{29}\text{Ni}_{29}\text{Zr}_7\text{B}_4\text{Cu}_1$  (at.%) were prepared by arc melting the mixtures of industrial pure Fe, Co, Ni, Zr, Cu metals and B crystals under Ti-gettered argon atmosphere. The ingots were re-melted 5 times to ensure chemical homogeneity. Ribbons were prepared by melt spinning with a copper wheel. The outer surface velocity of the wheel was about 32 m/s. The ribbons were sealed in evacuated quartz capsules for annealing treatment. In order to obtain better soft magnetic properties, the as-spun ribbons were annealed at  $350^\circ\text{C}$  for 10 min to release residual stress. Isothermally treatment was conducted at  $430^\circ\text{C}$  for various times. Non-isothermal crystallization sample was prepared by increasing temperature from room temperature to  $450^\circ\text{C}$ ,  $610^\circ\text{C}$  and  $800^\circ\text{C}$  respectively at heating rate of  $20^\circ\text{C}/\text{min}$  and then water-quenched.

Differential scanning calorimetry (SETARAM Labsys<sup>TM</sup> TG DSC) was used to investigate the thermal behavior and the crystallization kinetics of the ribbons at the heating rates of  $5^\circ\text{C}/\text{min}$ ,  $10^\circ\text{C}/\text{min}$ ,  $20^\circ\text{C}/\text{min}$  and  $40^\circ\text{C}/\text{min}$ . The structure was examined by X-ray diffraction (XRD) using D8advance with  $\text{Cu-K}\alpha$  radiation. The chemical uniformity was investigated using energy-dispersive X-ray spectroscopy (EDS). Saturation magnetization ( $B_s$ ) was measured by vibrating sample magnetometer (VSM) under a maximum applied field of 1000 kA/m. Coercivity ( $H_c$ ) was measured with a DC  $B$ - $H$  loop tracer under a field of 1000 kA/m.

The total energy and magnetic moment of  $\text{Fe}_{30}\text{Co}_{29}\text{Ni}_{29}\text{Zr}_7\text{B}_4\text{Cu}_1$  HEA were calculated by first-principles density functional theory (DFT) simulation at zero temperature. The input disordered structures of the amorphous (128 atoms), fcc (108 atoms) and bcc (128 atoms) were constructed by random distribution of atoms. Projector augmented wave (PAW) method by the Vienna *Ab initio* Simulation Package (VASP) was used to perform DFT simulation [19–21]. Exchange-correlation of electrons was described with the Perdew–Burke–Ernzerh (PBE) [22]. The Brillouin zone was sampled by a Gamma centered  $k$ -point mesh of  $3 \times 3 \times 3$  for all models. The convergence threshold for optimized configuration was set to be less than  $0.02$  eV/Å on each atom. The plane-wave energy cutoff was held constant at 400 eV. All structures were optimized first in the non-magnetic state, and then re-optimized considering spin polarization. Both atomic coordinates and lattice parameters of fcc and bcc phase were fully relaxed under zero pressure until the energy convergence reached  $1 \times 10^{-4}$  eV/at. The configuration reaching to the lowest energy was used for data analysis. The average magnetic momentum of atoms is equal to the total magnetic momentum divided by the number of atoms. The  $E_{bond}$  of each structure was obtained by using the following

equation

$$E_{bond} = E_{total} - E_{atom} \quad (1)$$

where,  $E_{total}$  is the total energy of the stable systems, and  $E_{atom}$  is the sum of the energies of all the atoms in the stable systems.

## 3. Results

Fig. 1a shows DSC curves of the  $\text{Fe}_{30}\text{Co}_{29}\text{Ni}_{29}\text{Zr}_7\text{B}_4\text{Cu}_1$  HEA ribbons at different heating rates. The ribbons exhibit two obviously exothermic peaks, confirming the amorphous structure of as-quenched ribbons and crystallization occurring through two stages. Interestingly, the DSC curves ( $20^\circ\text{C}/\text{min}$  and  $40^\circ\text{C}/\text{min}$ ) have an obvious endothermic phenomenon at about  $750^\circ\text{C}$ , implying the occurrence of a phase transition, which is similar to that in other HEAs [14,23]. The XRD patterns in Fig. 1b also confirmed the amorphous phase of the as-spun ribbons. According to DSC heating process, non-isothermal annealing was conducted to reveal the structure evolution of the amorphous-HEA, as shown in Fig. 1b. It can be seen that as the temperature increases, the amorphous phase will first crystallize into the bcc phase (first crystallization peak,  $450^\circ\text{C}$ ), and then residual amorphous phase crystallize into fcc phase (second crystallization peak,  $610^\circ\text{C}$ ), and finally almost completely into the fcc phase (beyond endothermic peaks,  $800^\circ\text{C}$ ). It should be noted that although the amorphous bcc-fcc transition has also occurred in  $\text{Fe}_{26.7}\text{Co}_{26.7}\text{Ni}_{26.6}\text{Si}_9\text{B}_{11}$  alloy, the FCC phase occurs at a higher temperature (beyond the heat absorption peak) [14]. The different behavior of the bcc-fcc transformation of the current  $\text{Fe}_{30}\text{Co}_{29}\text{Ni}_{29}\text{Zr}_7\text{B}_4\text{Cu}_1$  alloy compare to that of  $\text{Fe}_{26.7}\text{Co}_{26.7}\text{Ni}_{26.6}\text{Si}_9\text{B}_{11}$  in Ref. [14] might be because of their different chemical composition. The fcc Cu-clusters in  $\text{Fe}_{30}\text{Co}_{29}\text{Ni}_{29}\text{Zr}_7\text{B}_4\text{Cu}_1$  amorphous samples might facilitate the formation of the fcc phase at temperatures lower than endothermic peak, which is different from that of Cu-free elements in the  $\text{Fe}_{26.7}\text{Co}_{26.7}\text{Ni}_{26.6}\text{Si}_9\text{B}_{11}$  alloy. In any case, the micro-mechanism of this difference needs to be further studied.

But, the bcc  $\rightarrow$  fcc phase transformation in the present alloy is very similar to that in  $\text{Fe}_{44}\text{Co}_{44}\text{Zr}_7\text{B}_4\text{Cu}_1$  amorphous alloy [24]. In order to study the phase evolution from amorphous to bcc in detail, isothermally treatment at  $430^\circ\text{C}$  (first crystallization peak temperature) for various times were conducted. As the annealing time increases, the semi-high width of Bragg peak gradually decreases, indicating that nanocrystalline gradually precipitate in amorphous matrix. After annealing for 60 min, the Bragg peaks can be clearly attributed to bcc phase, which is the same as non-isothermal crystallization phase at  $450^\circ\text{C}$ . The grain size of bcc phase for each annealed sample is determined to be about 20 nm, according to the Scherer formula [25]. The EDS maps of the ribbons annealed at  $430^\circ\text{C}$  for 60min in Fig. 2 show that all elements are uniformly distributed, suggesting that the bcc solid solution is high entropy phase. In short,  $\text{Fe}_{30}\text{Co}_{29}\text{Ni}_{29}\text{Zr}_7\text{B}_4\text{Cu}_1$  HEA with amorphous, bcc, bcc + fcc and fcc structure were successfully produced respectively.

Fig. 3 shows the hysteresis loops of the  $\text{Fe}_{30}\text{Co}_{29}\text{Ni}_{29}\text{Zr}_7\text{B}_4\text{Cu}_1$  HEA in different structural states. The  $H_c$  (27–80 A/m) of the present HEA ribbons is significantly smaller than that (629 A/m) of the FeCoNiMnAl HEA [17], indicating better soft magnetic properties. The amorphous-HEA and fcc-HEA have the similar  $B_s$  value (115 emu/g), as shown in (Fig. 3a), which was similar to that in Fe-Co-Ni-Si-B-P HEA [23]. After bcc phase precipitate in amorphous matrix, its  $B_s$  value increase to 125 emu/g. The gradual increase of the bcc phase volume fraction makes the  $B_s$  value increase gradually (Fig. 3b). It is also found that the  $B_s$  value of bcc is higher than that of fcc in other HEAs [26]. In short, the  $B_s$  value of the present soft magnetic HEAs with bcc structure is higher than that of

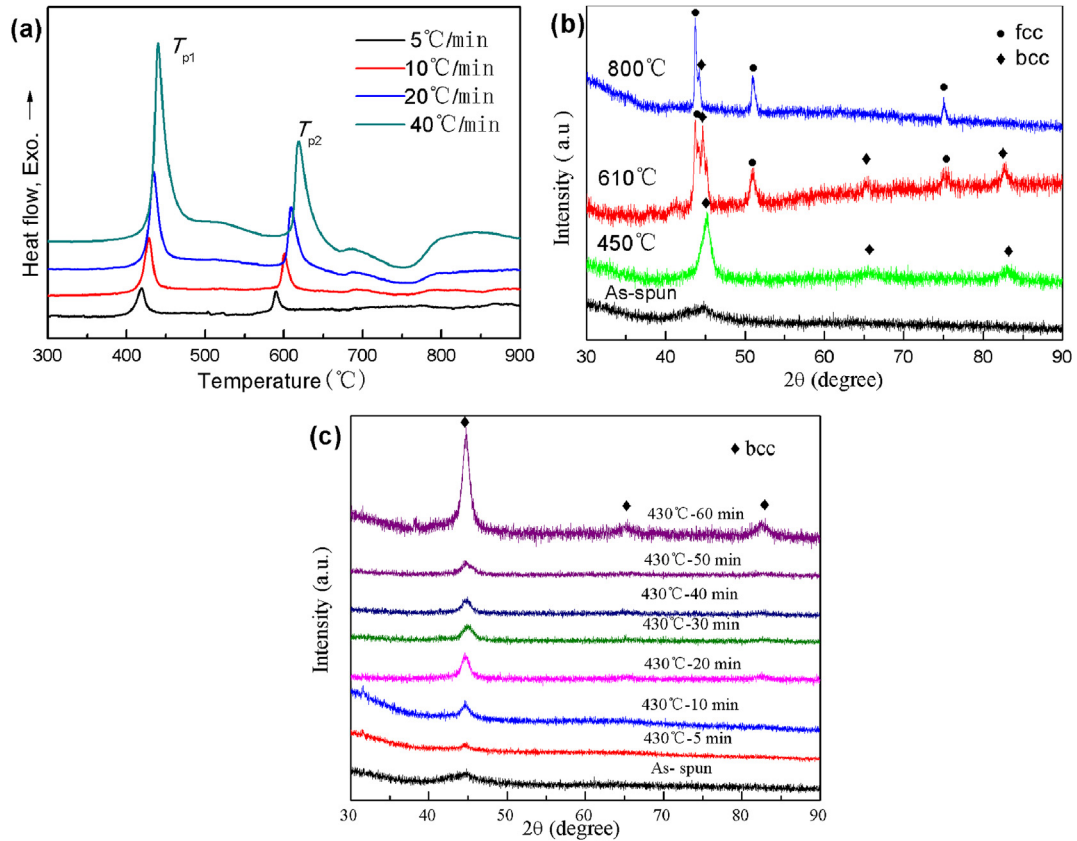


**Fig. 1.**  $\text{Fe}_{30}\text{Co}_{29}\text{Ni}_{29}\text{Zr}_7\text{B}_4\text{Cu}_1$  HEA: (a) DSC curves of the as-quenched amorphous ribbons at different heating rates, (b) XRD patterns of the as-quenched and after non-isothermal annealing ribbons, and (c) XRD patterns after isothermally treatment at  $430^\circ\text{C}$  for various times.

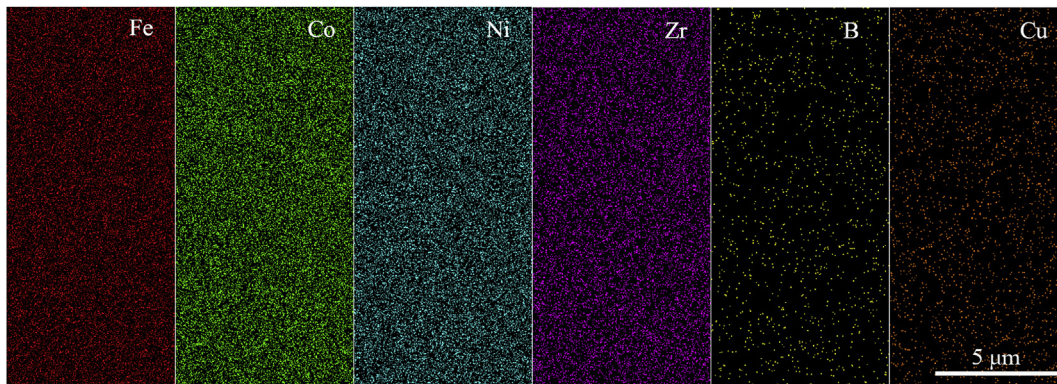


**Fig. 2.** EDS maps of the HEAs ribbons after annealing at  $430^\circ\text{C}$  for 60 min.

amorphous phase ( $\approx \text{fcc}$ ).

## 4. Discussion

### 4.1. Formation of amorphous phase and solid solution phase

In principle, any solid solution can become amorphous if sufficiently high cooling rate is given. However, most of amorphous-HEAs fail to form solid solution phase, and solid solution phase also fail to form amorphous phase using conventional cooling rate (melt-spinning or copper mold casting) [11]. It is believed that atomic size difference ( $\delta$ ) is the critical parameter that determines the formation solid solution or amorphous phases in HEAs [11].

Solid solution phases form when  $\delta \leq 8.5$ , while amorphous phases forms when  $\delta \geq 9$  [11]. The value of  $\delta$  for  $\text{Fe}_{30}\text{Co}_{29}\text{Ni}_{29}\text{Zr}_7\text{B}_4\text{Cu}_1$  HEA is 10. This HEA and our previous results [14,23] suggest that to design magnetic HEAs, in which both amorphous phase and solid solution phase can be formed, one should guarantee: (1) the  $\delta$  value around 10 and that the mixing enthalpy ( $\Delta H_{\text{mix}}$ ) simultaneously satisfy the formation range of amorphous phase and solid solution phase, and (2) adding a small amount of elements with small atomic size and low mixing enthalpy with Fe, Co and Ni, such as P, C, B etc., ensuring the alloy forms amorphous phase, and these small atoms would located in the lattice interstitial after the amorphous crystallization, and thus simple solid solution phase can be obtained. Anyhow, phase selection remains an open debate in HEAs.

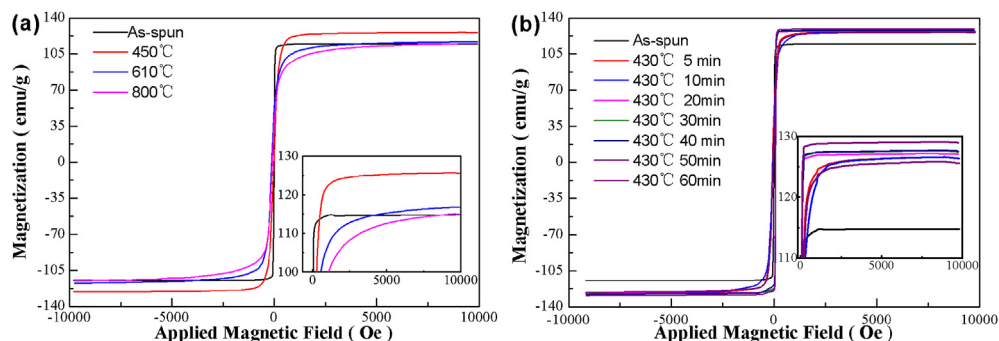


Fig. 3. Hysteresis loops of the  $\text{Fe}_{30}\text{Co}_{29}\text{Ni}_{29}\text{Zr}_7\text{B}_4\text{Cu}_1$  HEAs with different structures.

#### 4.2. Phase transformation from amorphous to bcc

It is well known that most crystallization products of high entropy amorphous alloys are intermetallics [27,28]. However, the crystallization products of the present HEA are simple solid solution phase. Because the composition of the solid solution phase and the amorphous matrix are almost identical, the crystallization process does not need long-term diffusion. The HEAs are chemically disordered alloy and have remarkable “sluggish diffusion effect”, which effectively impedes long-range diffusion [29]. It was reported that metastable B2-CuZr phase preferentially precipitate in  $\text{Cu}_{48}\text{Zr}_{48}\text{Al}_4$  amorphous matrix because of the composition similarity of B2-CuZr phase with the glassy phase [30]. Therefore, both low and high entropy amorphous alloys have non-long-term diffusion phenomenon during crystallization.

The barrier of each crystallization step can be evaluated by the activation energy. The activation energy of two exothermic peaks are calculated to be  $E_{p1} = 369.7$  kJ/mol and  $E_{p2} = 429.6$  kJ/mol respectively, by using Kissinger equation (Fig. 1a).  $E_{p2} > E_{p1}$  indicates that the first step crystallization is easier to occur, i.e., the first crystallization phase is bcc phase. The cohesive energy of amorphous, bcc and fcc phase were calculated by first-principles density functional theory (DFT), respectively. The cohesive energy of bcc phase is  $-662.3$  eV, which is very close to that ( $-662.8$  eV) of amorphous phase, while the fcc phase has relatively high cohesive energy of  $-557.9$  eV. Therefore, the energy barrier of amorphous  $\rightarrow$  bcc phase transformation is very low.

It can be speculated that the crystallization process of the present HEA was controlled by nucleation. Low level of Cu content usually promotes the precipitation of bcc-(Fe) or bcc-(Fe,Co) nanocrystalline in Fe- or (Fe,Co)-based amorphous alloys [31,32]. It was found that the fcc Cu-clusters in as-quenched amorphous samples are thermodynamically unstable, and begin to transform into bcc structure when the temperature is close to the crystallization temperature [32]. Note that Fe and FeCo have bcc structures. Simulation studies have found that FeCoNi alloy can also form bcc structure probably because of its configurational entropy change [33,34]. Thus, the bcc Cu-clusters can promote the nanocrystallization of the bcc solid solution in amorphous alloy. In addition, the density of amorphous alloys is lower than their crystalline counterparts [35]. The bcc structure of metallic materials has a much lower packing density ( $\sim 68\%$ ), compared with that of the fcc structures ( $\sim 74\%$ ), therefore, bcc structure with a lower density is expected through the optimal crystallization path. This specific feature should be investigated in detail in the future.

#### 4.3. Phase transformation from bcc to fcc

The bcc  $\rightarrow$  fcc phase transformation at about  $750^\circ\text{C}$  (see Fig. 1) is

similar to the transformation process of pure Fe or  $\text{Fe}_{44}\text{Co}_{44}\text{Zr}_7\text{B}_4\text{Cu}_1$  amorphous alloy from low temperature bcc to high temperature fcc [24]. A convenient framework for interpreting the transformation is provided by the energy landscape [36]. Compared to bcc phase, the higher cohesive energy reveals higher energy landscape of fcc phase. The energy provided by heating can overcome the energy barrier, making the present HEA to jump from low energy base (bcc) to high energy base (fcc). In order to further prove the existence of fcc phase at high temperature, we prepared a rod with diameter of 3 mm by copper casting, and found it has a single fcc structure, as shown in Fig. 4. Thus, the fcc phase can be kept to room temperature while the alloy melts are cooled.

#### 4.4. DFT calculations

The  $B_s$  was primarily determined by the composition and microstructure [15,17]. The addition of Al in CoFeMnNi HEA can facilitate the transformation of fcc to bcc, and much higher  $B_s$  was obtained [17]. While, the  $B_s$  value of the present HEAs is bcc  $>$  amorphous  $\approx$  fcc. To reveal the essential mechanism of this phenomenon, the DFT calculations were performed. The predicted local magnetic moments of individual atoms in fcc FeCoNi alloy, amorphous, bcc and fcc  $\text{Fe}_{44}\text{Co}_{44}\text{Zr}_7\text{B}_4\text{Cu}_1$  alloys at zero temperature are shown in Fig. 5. Average magnetic moments of composing elements are listed in Table 1. Fe, Co and Ni behave ferromagnetic-like in fcc FeCoNi alloy (Fig. 5a). Their spins are aligned perfectly and there is no scatter in magnetic moment distributions, which is very consistent with the results in Ref. [2]. This shows that our

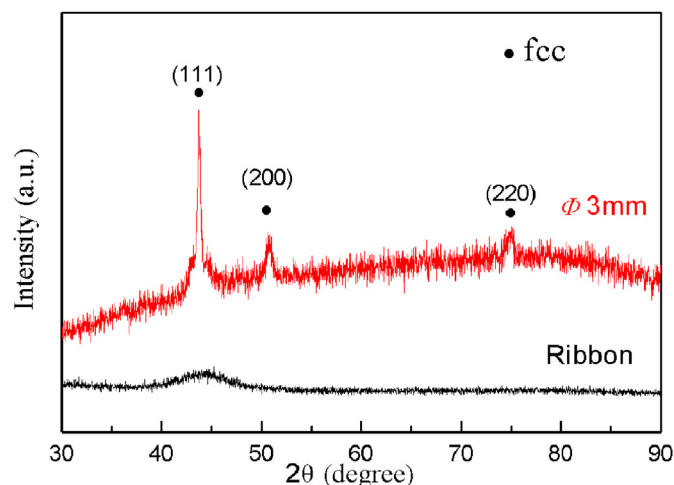


Fig. 4. XRD patterns of as-cast ribbon and rod of  $\text{Fe}_{30}\text{Co}_{29}\text{Ni}_{29}\text{Zr}_7\text{B}_4\text{Cu}_1$  alloy.

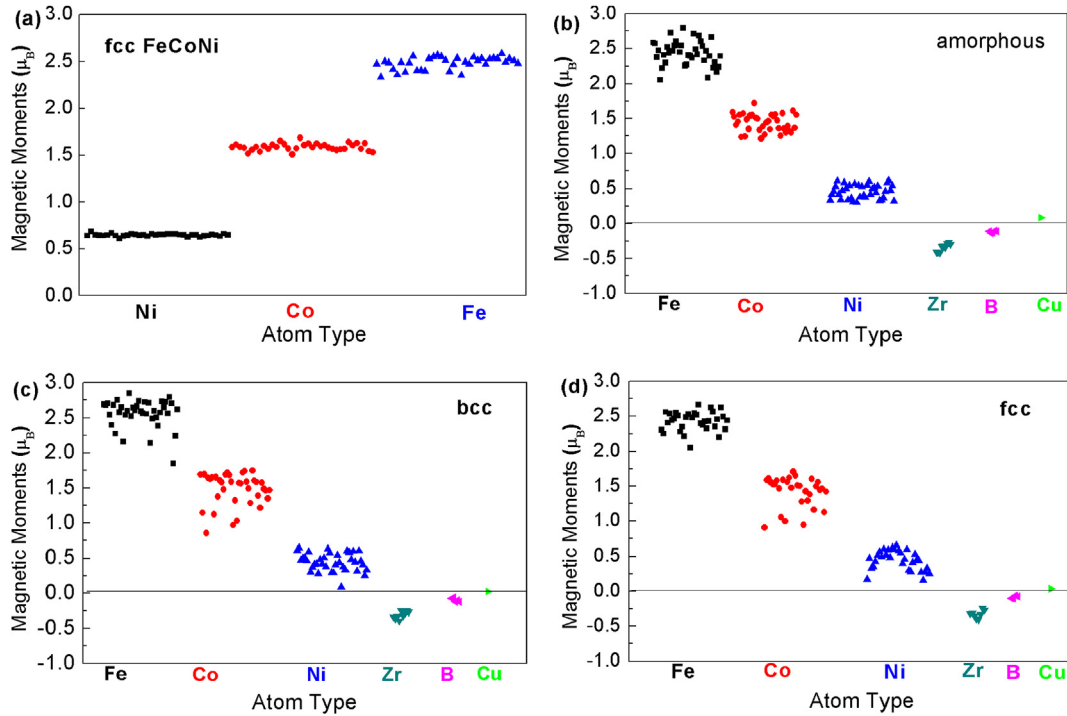


Fig. 5. Magnetic moments of individual atoms in fcc CoFeNi alloy (a), amorphous (b), bcc (c) and fcc (d)  $\text{Fe}_{44}\text{Co}_{44}\text{Zr}_7\text{B}_4\text{Cu}_1$  alloys predicted from DFT calculations at zero temperature.

**Table 1**  
Average magnetic moments of composing elements ( $\mu_B/\text{atom}$ ).

	Fe	Co	Ni	Zr	B	Cu
amorphous	2.4367	1.4382	0.4586	-0.341	-0.1164	0.087
bcc	2.5652	1.4862	0.4449	-0.3099	-0.0964	0.025
fcc	2.4284	1.4208	0.4555	-0.3114	-0.0742	0.032
fcc FeCoNi	2.4819	1.5867	0.6476	—	—	—

simulation method is feasible. The addition of Zr, B and Cu to FeCoNi causes larger scattering in the moment of the ferromagnetic atoms (Fig. 5 b, c and d), suggesting the sensitivity of the magnetic moment to neighboring atoms. Zr and B are antiferromagnetic elemental in  $\text{Fe}_{30}\text{Co}_{29}\text{Ni}_{29}\text{Zr}_7\text{B}_4\text{Cu}_1$  HEA, as their magnetic moments have negative values, while magnetic moment of Cu is zero. But the average magnetic moments of Fe in bcc is higher than that in amorphous or fcc. In conclusion, the calculated results are consistent with the experimental results in the trend.

## 5. Conclusion

In order to study the effect of structure on soft-magnetic properties and exclude the interference of composition,  $\text{Fe}_{30}\text{Co}_{29}\text{Ni}_{29}\text{Zr}_7\text{B}_4\text{Cu}_1$  HEA with amorphous, bcc and fcc structure were successfully produced respectively. We explained the mechanism of phase transitions. The amorphous and fcc phase have the similar  $B_s$  value. After bcc phase precipitate in amorphous matrix, the  $B_s$  of the alloy slightly increased. An important consequence of this paper is that we offer a prototype to study the phase formation mechanism, the correlation between phase and magnetic properties and how to design high performance HEAs.

## Acknowledgements

This work was supported by the National Natural Science

Foundation of China (Grant Nos. U1704159 and 51701183) and China Postdoctoral Science Foundation (Grant No. 2018M630834).

## References

- [1] F.X. Zhang, S. Zhao, K. Jin, H. Bei, D. Popov, C. Park, J.C. Neuefeind, W.J. Weber, Y. Zhang, Pressure-induced fcc to hcp phase transition in Ni-based high entropy solid solution alloys, *Appl. Phys. Lett.* 110 (2017), 011902. <https://doi.org/10.1063/1.4973627>.
- [2] C. Niu, C.R. LaRosa, J. Miao, M.J. Mills, M. Ghazisaeidi, Magnetically-driven phase transformation strengthening in high entropy alloys, *Nat. Commun.* 9 (2018) 1363. <https://doi.org/10.1038/s41467-018-03846-0>.
- [3] F. Zhang, Y. Wu, H. Lou, Z. Zeng, V.B. Prakapenka, E. Greenberg, Y. Ren, J. Yan, J.S. Okasinski, X. Liu, Y. Liu, Q. Zeng, Z. Lu, Polymorphism in a high-entropy alloy, *Nat. Commun.* 8 (2017) 15687. <https://doi.org/10.1038/ncomms15687>.
- [4] B. Cheng, F. Zhang, H. Lou, X. Chen, P.K. Liaw, J. Yan, Z. Zeng, Y. Ding, Q. Zeng, Pressure-induced phase transition in the AlCoCrFeNi high-entropy alloy, *Scripta Mater.* 161 (2019) 88–92. <https://doi.org/10.1016/j.scriptamat.2018.10.020>.
- [5] C.S. Yoo, H. Cynn, P. Söderlind, V. Iota, New  $\beta(\text{fcc})$ -Cobalt to 210 GPa, *Phys. Rev. Lett.* 84 (2000) 4132–4135. <https://doi.org/10.1103/PhysRevLett.84.4132>.
- [6] H.W. Sheng, H.Z. Liu, Y.Q. Cheng, J. Wen, P.L. Lee, W.K. Luo, S.D. Shastri, E. Ma, Polymorphism in a metallic glass, *Nat. Mater.* 6 (2007) 192. <https://doi.org/10.1038/nmat1839>.
- [7] Q. Zeng, H. Sheng, Y. Ding, L. Wang, W. Yang, J.-Z. Jiang, W.L. Mao, H.-K. Mao, Long-range topological order in metallic glass, *Science* 332 (2011) 1404–1406. <https://doi.org/10.1126/science.1200324>.
- [8] Z.H. Han, S. Liang, J. Yang, R. Wei, C.J. Zhang, A superior combination of strength-ductility in CoCrFeNiMn high-entropy alloy induced by asymmetric rolling and subsequent annealing treatment, *Mater. Char.* 145 (2018) 619–626. <https://doi.org/10.1016/j.matchar.2018.09.029>.
- [9] S. Wei, F. He, C.C. Tasan, Metastability in high-entropy alloys: a review, *J. Mater. Res.* 33 (2018) 2924–2937. <https://doi.org/10.1557/jmr.2018.306>.
- [10] L.B. Chen, R. Wei, K. Tang, J. Zhang, F. Jiang, L. He, J. Sun, Heavy carbon alloyed FCC-structured high entropy alloy with excellent combination of strength and ductility, *Mater. Sci. Eng., A* 716 (2018) 150–156. <https://doi.org/10.1016/j.msea.2018.01.045>.
- [11] S. Guo, C.T. Liu, Phase stability in high entropy alloys: formation of solid-solution phase or amorphous phase, *Prog. Nat. Sci. Mater.* 21 (2011) 433–446. [https://doi.org/10.1016/s1002-0071\(12\)60080-x](https://doi.org/10.1016/s1002-0071(12)60080-x).
- [12] M.C. Gao, D.B. Miracle, D. Maurice, X. Yan, Y. Zhang, J.A. Hawk, High-entropy functional materials, *J. Mater. Res.* 33 (2018) 3138–3155. <https://doi.org/10.1557/jmr.2018.323>.
- [13] R. Wei, J. Tao, H. Sun, C. Chen, G.W. Sun, F.S. Li, Soft magnetic

- Fe<sub>26.7</sub>Co<sub>26.7</sub>Ni<sub>26.6</sub>Si<sub>9</sub>B<sub>11</sub> high entropy metallic glass with good bending ductility, *Mater. Lett.* 197 (2017) 87–89. <https://doi.org/10.1016/j.matlet.2017.03.159>.
- [14] R. Wei, H. Sun, C. Chen, J. Tao, F. Li, Formation of soft magnetic high entropy amorphous alloys composites containing in situ solid solution phase, *J. Magn. Mater.* 449 (2018) 63–67. <https://doi.org/10.1016/j.jmmm.2017.09.065>.
- [15] Z. Li, H. Xu, Y. Gu, M. Pan, L. Yu, X. Tan, X. Hou, Correlation between the magnetic properties and phase constitution of FeCoNi(CuAl)<sub>0.8</sub>Gax (0 < x < 0.08) high-entropy alloys, *J. Alloys Compd.* 746 (2018) 285–291. <https://doi.org/10.1016/j.jallcom.2018.02.189>.
- [16] P. Li, A. Wang, C.T. Liu, Composition dependence of structure, physical and mechanical properties of FeCoNi(MnAl) x high entropy alloys, *Intermetallics* 87 (2017) 21–26. <https://doi.org/10.1016/j.intermet.2017.04.007>.
- [17] T. Zuo, M.C. Gao, L. Ouyang, X. Yang, Y. Cheng, R. Feng, S. Chen, P.K. Liaw, J.A. Hawk, Y. Zhang, Tailoring magnetic behavior of CoFeMnNi<sub>x</sub> (X=Al, Cr, Ga, and Sn) high entropy alloys by metal doping, *Acta Mater.* 130 (2017) 10–18. <https://doi.org/10.1016/j.actamat.2017.03.013>.
- [18] L.B. Chen, R. Wei, K. Tang, J. Zhang, F. Jiang, J. Sun, Ductile-brittle transition of carbon alloyed Fe<sub>40</sub>Mn<sub>40</sub>Co<sub>10</sub>Cr<sub>10</sub> high entropy alloys, *Mater. Lett.* 236 (2019) 416–419. <https://doi.org/10.1016/j.matlet.2018.10.144>.
- [19] B. PE, Projector augmented-wave method, *Phys. Rev. B* 50 (1994) 17953–17979. <https://doi.org/10.1103/PhysRevB.50.17953>.
- [20] G. Kresse, J. Furthmüller, Efficient iterative schemes for ab initio total-energy calculations using a plane-wave basis set, *Phys. Rev. B* 54 (1996) 11169–11186. <https://doi.org/10.1103/physrevb.54.11169>.
- [21] G. Kresse, J. Furthmüller, Efficiency of ab-initio total energy calculations for metals and semiconductors using a plane-wave basis set, *Comput. Mater. Sci.* 6 (1996) 15–50. [https://doi.org/10.1016/0927-0256\(96\)00008-0](https://doi.org/10.1016/0927-0256(96)00008-0).
- [22] J.P. Perdew, K. Burke, M. Ernzerhof, Generalized gradient approximation made simple, *Phys. Rev. Lett.* 77 (1996) 3865–3868. <https://doi.org/10.1103/PhysRevLett.77.3865>.
- [23] R. Wei, H. Sun, C. Chen, Z. Han, F. Li, Effect of cooling rate on the phase structure and magnetic properties of Fe 26.7 Co 28.5 Ni 28.5 Si 4.6 B 8.7 P 3 high entropy alloy, *J. Magn. Mater.* 435 (2017) 184–186. <https://doi.org/10.1016/j.jmmm.2017.04.017>.
- [24] M.A. Willard, M.Q. Huang, D.E. Laughlin, M.E. McHenry, J.O. Cross, V.G. Harris, C. Franchetti, Magnetic properties of HITPERM (Fe, Co)<sub>88</sub>Zr<sub>7</sub>B<sub>4</sub>Cu<sub>1</sub> magnets, *J. Appl. Phys.* 85 (1999) 4421–4423. <https://doi.org/10.1063/1.369804>.
- [25] Y. Han, R. Wei, Z. Li, F. Li, A. Wang, C. Chang, X. Wang, Improvement of magnetic properties for V-substituted Fe<sub>73.5</sub>Si<sub>13.5</sub>B<sub>9</sub>Cu<sub>1</sub>Nb<sub>3-x</sub>V<sub>x</sub> nanocrystalline alloys, *J. Mater. Sci. Mater. Electron.* 28 (2017) 10555–10563. <https://doi.org/10.1007/s10854-017-6829-2>.
- [26] Z. Li, Y. Gu, C. Wang, M. Pan, H. Zhang, Z. Wu, X. Hou, X. Tan, H. Xu, Microstructure and magnetic properties of the FeCoNi(CuAl)<sub>0.8</sub>Ga<sub>0.06</sub> high-entropy alloy during the phase transition, *J. Alloys Compd.* 779 (2019) 293–300. <https://doi.org/10.1016/j.jallcom.2018.11.235>.
- [27] J. Kim, H.S. Oh, J. Kim, C.W. Ryu, G.W. Lee, H.J. Chang, E.S. Park, Utilization of high entropy alloy characteristics in Er-Gd-Y-Al-Co high entropy bulk metallic glass, *Acta Mater.* 155 (2018) 350–361. <https://doi.org/10.1016/j.actamat.2018.06.024>.
- [28] Y. Li, W. Zhang, T. Qi, New soft magnetic Fe<sub>25</sub>Co<sub>25</sub>Ni<sub>25</sub>(P,C,B)<sub>25</sub> high entropy bulk metallic glasses with large supercooled liquid region, *J. Alloys Compd.* 693 (2017) 25–31. <https://doi.org/10.1016/j.jallcom.2016.09.144>.
- [29] K.Y. Tsai, M.H. Tsai, J.W. Yeh, Sluggish diffusion in Co–Cr–Fe–Mn–Ni high-entropy alloys, *Acta Mater.* 61 (2013) 4887–4897. <https://doi.org/10.1016/j.actamat.2013.04.058>.
- [30] R. Wei, X.L. Wang, S. Yang, F. Jiang, L. He, Formation of CuZr-based bulk metallic glass composites containing nanometer-scale B2–CuZr phase through sub-Tg annealing, *J. Alloys Compd.* 617 (2014) 699–706. <https://doi.org/10.1016/j.jallcom.2014.08.045>.
- [31] M. Stoica, P. Ramasamy, I. Kaban, S. Scudino, M. Nicoara, G.B.M. Vaughan, J. Wright, R. Kumar, J. Eckert, Structure evolution of soft magnetic (Fe<sub>36</sub>Co<sub>36</sub>B<sub>19.2</sub>Si<sub>4.8</sub>Nb<sub>4</sub>)<sub>100-x</sub>Cu<sub>x</sub> (x = 0 and 0.5) bulk glassy alloys, *Acta Mater.* 95 (2015) 335–342. <https://doi.org/10.1016/j.actamat.2015.05.042>.
- [32] M. Nishijima, M. Matsuura, K. Takenaka, A. Takeuchi, H. Ofuchi, A. Makino, Phase transition from fcc to bcc structure of the Cu-clusters during nanocrystallization of Fe<sub>85.2</sub>Si<sub>1</sub>B<sub>9</sub>P<sub>4</sub>Cu<sub>0.8</sub> soft magnetic alloy, *AIP Adv.* 4 (2014), 6044–6041, <https://doi.org/10.1063/1.4880241>.
- [33] G. Anand, R. Goodall, C.L. Freeman, Role of configurational entropy in body-centred cubic or face-centred cubic phase formation in high entropy alloys, *Scripta Mater.* 124 (2016) 90–94. <https://doi.org/10.1016/j.scriptamat.2016.07.001>.
- [34] S. Huang, E. Holmström, O. Eriksson, L. Vitos, Mapping the magnetic transition temperatures for medium- and high-entropy alloys, *Intermetallics* 95 (2018) 80–84. <https://doi.org/10.1016/j.intermet.2018.01.016>.
- [35] Y. Li, Q. Guo, J.A. Kalb, C.V. Thompson, Matching glass-forming ability with the density of the amorphous phase, *Science* 322 (2008) 1816–1819. <https://doi.org/10.1126/science.1163062>.
- [36] M. Jafary-Zadeh, Z.H. Aitken, R. Tavakoli, Y.-W. Zhang, On the controllability of phase formation in rapid solidification of high entropy alloys, *J. Alloys Compd.* 748 (2018) 679–686. <https://doi.org/10.1016/j.jallcom.2018.03.165>.